ORIGINAL ARTICLE

Fuzzy Adaptive State Estimation of Distributed Drive Electric Vehicles with Random Missing Measurements and Unknown Process Noise

Zhiguo Zhang[1], Guodong Yin[1], Chao Huang[2], Jingyu Hu[1], Xing Xu[3], Chengyue Jiang[4] and Yan Wang[2*]

Abstract

Accurate estimation of sideslip angle and vehicle velocity is crucial for effective control of distributed drive electric vehicles. However, as these states are not directly measured, Kalman-based approaches utilizing in-vehicle sensors have been developed to estimate them. Unfortunately, existing methods tend to ignore the impact of data loss on estimation performance. Furthermore, the process noise, which changes dynamically due to varying driving conditions, is not adequately considered. In response to these constraints, we propose a novel method called the fuzzy adaptive fault-tolerant extended Kalman filter (FAFTEKF). Initially, a fault-tolerant EKF is devised to handle missing measurements. Additionally, a fuzzy logic system that dynamically updates the process noise matrix, is built to improve estimation accuracy under different driving conditions. Extensive experimental results validate the superiority of the FAFTEKF over the traditional EKF across various scenarios with different degrees of data loss.

Keywords Distributed drive electric vehicles, State estimation, Fault-tolerant EKF, Fuzzy logic system

1 Introduction

Traffic accidents have always been a major cause of significant casualties and economic losses [1]. To mitigate these issues, extensive efforts have been made to develop autonomous driving systems and advance chassis control systems [2, 3]. In complex traffic scenarios, motion state estimation of vehicles plays a vital role in enabling autonomous driving [4, 5]. Once a high-level driving decision has been made, distributed drive electric vehicles (DDEV) will execute some control commands based on some key information on the vehicle state [6]. Among various influential factors, the accurate estimation of vehicle states, particularly sideslip angle and vehicle velocity, is crucial during vehicle control. However, directly measuring these key states using onboard sensors remains challenging. Therefore, the research focus is currently on developing methods to estimate these vehicle states solely based on onboard sensor data.

Recently, a variety of techniques have been employed for vehicle state estimation. Zhang et al. [7] devised an H infinity observer to forecast the sideslip angle using front-wheel angle data. The controller output observer [8] has been explored for estimating tire and traction forces separately. Zhao et al. [9] introduced a nonlinear observer for vehicle velocity estimation, demonstrating superior performance in certain tests compared to a linear observer. Gao et al. [10] formulated a high-gain nonlinear observer for sideslip angle estimation. Among these methods, the sliding mode observer (SMO) is widely adopted. Variants like the reduced-order SMO [11] and higher-order SMO

*Correspondence:
Yan Wang
yanjack.wang@polyu.edu.hk
[1] School of Mechanical Engineering, Southeast University, Nanjing 211189, China
[2] Department of Industrial and System Engineering, The Hong Kong Polytechnical University, Hong Kong, China
[3] Department of Automotive Engineering Research Institute, Jiangsu University, Zhenjiang 225009, China
[4] College of Vehicle Engineering, Chongqing University of Technology, Chongqing 400054, China

Zhang *et al. Chinese Journal of Mechanical Engineering*   (2024) 37:118

Page 2 of 12

[12] have emerged for enhanced vehicle state estimation. Nonetheless, the accuracy of these observer-based techniques heavily depends on precise vehicle models, which are often challenging to acquire in practical scenarios.

Unlike observer-based methods, the Kalman filter algorithm and its variations are highly effective in achieving minimum mean squared error estimates when dealing with Gaussian noise. Consequently, Kalman-based approaches have gained extensive traction in vehicle state estimation. Within this domain, the extended Kalman filter (EKF) emerges as a favored option. In their work, Wenzel et al. [13] introduced a dual EKF estimation framework for predicting vehicle state, which addresses both parameter identification and state estimation problems. Baffet et al. [14] developed an EKF-based estimator specifically for predicting sideslip angle. Doumiati et al. [15] employed the EKF for the prediction of both sideslip angle and lateral tire forces. Meanwhile, Nam et al. [16] applied the EKF to a real vehicle for predicting sideslip angle using tire force sensor data. Additionally, to improve the robustness of the EKF, an extended H-infinity Kalman filter was introduced in [17]. Furthermore, the interacting multiple model EKF was utilized for vehicle state prediction [18]. Apart from the sideslip angle, it is also crucial to dynamically predict the vehicle velocity. Guo et al. [19] devised an EKF to estimate vehicle velocity using a field-programmable gate array, demonstrating high computational efficiency in test results. Katriniok et al. [20] presented a kinematics-based estimation method for predicting vehicle velocity. Additionally, Zhang et al. [21] developed an adaptive Kalman filter for predicting vehicle velocity and the experimental results proved the superiority of the proposed method. Similar studies have been reported [22].

While there have been significant research achievements in estimating vehicle state using the EKF, many of these studies fail to consider the impact of missing measurements. In practice, sensor data is often incomplete [23]. In response to this challenge, a robust EKF approach was proposed [24] to estimate vehicle state in the presence of missing measurements. This method enhances estimation performance specifically when data loss follows a uniform distribution. Similar investigations have been reported [25]. Additionally, real-time changes in vehicle dynamics due to varying driving conditions such as icy roads, snowy roads, and asphalt roads introduce time-varying process noise. However, most prior research assumes the process noise matrix is known, which leads to decreased estimation performance in complex driving conditions.

Based on the preceding discourse, a novel approach called the fuzzy adaptive fault-tolerant extended Kalman filter (FAFTEKF) has been devised to address the challenges of measurement loss and unknown process noise. This method

consists of two fundamental components: the fault-tolerant extended Kalman filter (FTEKF) and the fuzzy logic system. The FTEKF serves to mitigate the impact of missing measurements on estimation accuracy. Additionally, a dynamic fuzzy logic system has been developed to update the process noise matrix, thereby enhancing the adaptability of the FTEKF. The key contributions of this approach can be summarized as follows.

(1) A novel FAFTEKF is proposed to estimate vehicle state in case of data loss and unknown process noise. The FAFTEKF algorithm combines the FTEKF with a fuzzy logic system, enabling improved estimation performance in diverse working conditions.
(2) Comprehensive simulations and real vehicle experiments are conducted to validate the effectiveness of the FAFTEKF. The experimental results provide compelling evidence of the algorithm's capability to accurately estimate the sideslip angle and vehicle velocity, reinforcing its practical viability.

The paper is structured as follows. Section 2 provides an overview of the vehicle model used in this study. In Section 3, the details of the FAFTEKF approach are presented. The simulation and experimental results are discussed in Section 4. Finally, Section 5 concludes the paper by summarizing the main findings and highlighting future research directions.

2 Vehicle Model and Problem Formulation

We have chosen the four-wheel vehicle model [26] as a representation of the vehicle's dynamic response. The diagram of this model can be seen in Figure 1. The precise mathematical equations for this model are provided in Eqs. (1)–(4).

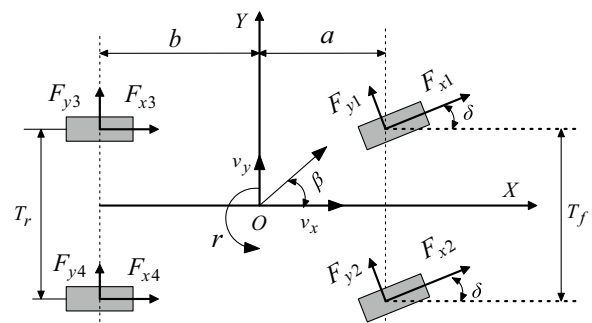$$m(\dot{v}_x - rv_y) = (F_{x1}+F_{x2}) \cos \delta + F_{x3} + F_{x4} - (F_{y1} + F_{y2}) \sin \delta, \tag{1}$$

Figure 1 The four-wheel model

Zhang et al. Chinese Journal of Mechanical Engineering   (2024) 37:118

Page 3 of 12

$$m(\dot{v}_y + rv_x) = (F_{x1}+F_{x2})\sin\delta + F_{y3} + F_{y4} + (F_{y1} + F_{y2})\cos\delta, \tag{2}$$

$$\dot{r} = \{a[(F_{x1} + F_{x2})\sin\delta + (F_{y1} + F_{y2})\cos\delta] - b(F_{y3} + F_{y4})\}/I_z, \tag{3}$$

$$J_i\dot{\omega}_t = T_{di} - T_{bi} - L_iF_{xi} \quad i = 1, 2, 3, 4, \tag{4}$$

where $i = 1, 2, 3, 4$, which correspond to the left-front, right-front, left-rear, and right-rear wheels, respectively. a and b denote the distances from the center of gravity to the front and rear axles. F_{xi}, F_{yi} represent longitudinal and lateral tire forces, respectively. r, m represent the yaw rate and vehicle mass, respectively. T_f and T_r represent the front and rear track widths. δ denotes the front wheel angle. v_x, v_y, β represent longitudinal vehicle velocity, lateral vehicle velocity, and sideslip angle, respectively. I_z denotes the moment of inertia about the vehicle's vertical axis. ω_i represents the wheel rotational speed; L_i is the wheel radius; T_{bi}, T_{di}, J_i denote the braking torque, driving torque, and moment of inertia, respectively.

We utilize a brushed tire model [27] to depict the dynamic characteristics of tires. The following equations outline specific aspects

$$F_{x,i} = \frac{C_x\left(\frac{s_i}{1+s_i}\right)}{f_i}F_i, \tag{5}$$

$$F_{y,i} = -\frac{C_y\left(\frac{\tan\alpha_i}{1+s_i}\right)}{f_i}F_i, \tag{6}$$

$$F_i = \begin{cases} f_i - \dfrac{1}{3\mu F_{z,i}}f_i^2 + \dfrac{1}{27\mu^2 F_{z,i}^2}f_i^3, & \text{if } f_i \le 3\mu F_{z,i}, \\ \mu F_{z,i}, & \text{else}, \end{cases} \tag{7}$$

$$f_i = \sqrt{C_x^2\left(\frac{s_i}{1+s_i}\right)^2 + C_y^2\left(\frac{\tan\alpha_i}{1+s_i}\right)^2}, \tag{8}$$

$$F_{z,1} = \frac{mgb}{2(a+b)} - \frac{ma_xh}{2(a+b)} - \frac{ma_yh}{T_f}\cdot\frac{b}{a+b}, \tag{9}$$

$$F_{z,2} = \frac{mgb}{2(a+b)} - \frac{ma_xh}{2(a+b)} + \frac{ma_yh}{T_f}\cdot\frac{b}{a+b}, \tag{10}$$

$$F_{z,3} = \frac{mga}{2(a+b)} + \frac{ma_xh}{2(a+b)} - \frac{ma_yh}{T_r}\cdot\frac{a}{a+b}, \tag{11}$$

$$F_{z,4} = \frac{mga}{2(a+b)} + \frac{ma_xh}{2(a+b)} + \frac{ma_yh}{T_r}\cdot\frac{a}{a+b}, \tag{12}$$

$$s_i = \text{sgn}(v_x - L_iw_i)\frac{|v_x - L_iw_i|}{\max(L_iw_i, v_x)}, \tag{13}$$

$$\alpha_1 = \delta - \arctan\left(\frac{v_y + ar}{v_x - T_fr/2}\right), \tag{14}$$

$$\alpha_2 = \delta - \arctan\left(\frac{v_y + ar}{v_x + T_fr/2}\right), \tag{15}$$

$$\alpha_3 = -\arctan\left(\frac{v_y - br}{v_x - T_rr/2}\right), \tag{16}$$

$$\alpha_4 = -\arctan\left(\frac{v_y - br}{v_x + T_rr/2}\right), \tag{17}$$

where a_x and a_y represent longitudinal and lateral accelerations;h denotes the height of the center of gravity; μ is tire-road friction coefficient; C_x, C_y, $F_{z,i}$ denote the longitudinal, lateral stiffness coefficients, and vertical tire forces, respectively; s_i, α_i stand for the longitudinal slip ratio and wheel sideslip angle; $i = 1, 2, 3, 4$, it shares the same physical significance as the vehicle model.

Based on the aforementioned equations, we have established a discrete vehicle state-space model that incorporates missing measurements. The model is as follows.

$$\begin{cases} \chi_{\tau+1} = \Gamma(\chi_\tau, u_\tau) + \psi_\tau, \\ z_\tau = \Pi_\tau h(\chi_\tau, u_\tau) + \varsigma_\tau, \end{cases} \tag{18}$$

$$\begin{cases} \chi_\tau = [v_x, v_y, r]^{\mathrm{T}}, \\ z_\tau = [r, a_x, a_y]^{\mathrm{T}}, \\ u_\tau = [\delta]^{\mathrm{T}}. \end{cases}$$

The process noise denoted as ψ_τ, has a covariance of Ω_τ. Similarly, the measurement noise denoted as ς_τ, has a covariance of R_τ. τ represents the sampling instant; the measurement vector is z_τ; the state transition function is denoted as Γ; the input vector is u_τ. Additionally, the measurement output function is h. The state vector is denoted as χ_τ, and it is important to note that the process noise and measurement noise are uncorrelated. $\Pi_\tau = \text{diag}\{\varepsilon_\tau^1, \varepsilon_\tau^2, \cdots, \varepsilon_\tau^n\}$, where $\varepsilon_\tau^i (i = 1, 2, \cdots, n)$ denotes n independent random variables and is not related to any noise signals. $\text{diag}\{\cdot\}$ is a diagonal matrix, and the probability density function is represented as ε_τ^i. Furthermore, it should be noted that the initial state χ_0 is also not related to any noise signals.

3 Methodology

In this section, we present the flowchart of the vehicle state estimation process based on the FAFTEKF, as shown in Figure 2. The FTEKF calculates the prior vehicle state, followed by the computation of the prior covariance using the updated process noise. The fuzzy system utilizes longitudinal and lateral acceleration and yaw rate information to update the process noise. Subsequently, the posterior vehicle state is updated using Eq. (20). Finally, Eq. (29) is employed to update the posterior covariance. These iterative steps are continuously cycled to ensure an accurate estimation of the vehicle state. Initially, we introduce the iterative formulation of the FTEKF. Subsequently, we integrate a fuzzy logic system to enhance the adaptability of the FTEKF.

3.1 The FTEKF

Within the framework of the traditional EKF, the recursive filtering can be expressed as follows:

$$\hat{\chi}_{\tau+1}^- = \Gamma(\hat{\chi}_\tau^-, u_\tau), \tag{19}$$

$$\hat{\chi}_{\tau+1}^+ = \hat{\chi}_{\tau+1}^- + M_{\tau+1}\left[z_{\tau+1} - \overline{\Pi}_{\tau+1}h(\hat{\chi}_{\tau+1}^-, u_{\tau+1})\right], \tag{20}$$

where $M_{\tau+1}$ is a filter gain, $\overline{\Pi}_{\tau+1} = \mathrm{E}(\Pi_{\tau+1})$.

Let us define the posterior state prediction error as $\omega_{\tau+1}^+ = \chi_{\tau+1} - \hat{\chi}_{\tau+1}^+$ and the prior state prediction error as $\omega_{\tau+1}^- = \chi_{\tau+1} - \hat{\chi}_{\tau+1}^-$. By combining Eqs. (18), (19), and (20), we obtain Eqs. (21) and (22).

$$\omega_{\tau+1}^- = \Gamma(\chi_\tau, u_\tau) + \psi_\tau - \Gamma(\hat{\chi}_\tau^+, u_\tau), \tag{21}$$

$$\omega_{\tau+1}^+ = \Gamma(\chi_\tau, u_\tau) + \psi_\tau - \hat{\chi}_{\tau+1}^- \\ - M_{\tau+1}\left[z_{\tau+1} - \overline{\Pi}_{\tau+1}h(\hat{\chi}_{\tau+1}^-, u_{\tau+1})\right], \tag{22}$$

To linearize the $\Gamma(\chi_\tau, u_\tau)$ and $h(\chi_{\tau+1}, u_{\tau+1})$, we utilize a first-order Taylor series expansion and disregard the higher-order terms.

$$\Gamma(\chi_\tau, u_\tau) = \Gamma(\hat{\chi}_\tau^+, u_\tau) + \left.\frac{\partial \Gamma(\chi_\tau, u_\tau)}{\partial \chi_\tau}\right|_{\chi_\tau = \hat{\chi}_\tau^+} \omega_\tau^+, \tag{23}$$

$$\omega_{\tau+1}^- = \left.\frac{\partial \Gamma(\chi_\tau, u_\tau)}{\partial \chi_\tau}\right|_{\chi_\tau = \hat{\chi}_\tau^+} \omega_\tau^+ + \psi_\tau, \tag{24}$$

$$h(\chi_{\tau+1}, u_{\tau+1}) = h(\hat{\chi}_{\tau+1}^-, u_{\tau+1}) + \left.\frac{\partial h(\chi_{\tau+1}, u_{\tau+1})}{\partial \chi_{\tau+1}}\right|_{\chi_{\tau+1} = \hat{\chi}_{\tau+1}^-} \omega_{\tau+1}^-, \tag{25}$$

$$\begin{aligned} \omega_{\tau+1}^+ &= \Gamma(\hat{\chi}_\tau^+, u_\tau) + \left.\frac{\partial \Gamma(\chi_\tau, u_\tau)}{\partial \chi_\tau}\right|_{\chi_\tau = \hat{\chi}_\tau^+} \omega_\tau^+ + \psi_\tau - \Gamma(\hat{\chi}_\tau^+, u_\tau) \\ &\quad - M_{\tau+1}\left[\begin{matrix} (\Pi_{\tau+1} - \bar{\Pi}_{\tau+1})h(\hat{\chi}_{\tau+1}^-, u_{\tau+1}) \\ + \varsigma_{\tau+1} + \Pi_{\tau+1}\left.\frac{\partial h(\chi_{\tau+1}, u_{\tau+1})}{\partial \chi_{\tau+1}}\right|_{\chi_{\tau+1} = \hat{\chi}_{\tau+1}^-} \omega_{\tau+1}^- \end{matrix}\right] \\ &= (I - M_{\tau+1}\Pi_{\tau+1}\left.\frac{\partial h(\chi_{\tau+1}, u_{\tau+1})}{\partial \chi_{\tau+1}}\right|_{\chi_{\tau+1} = \hat{\chi}_{\tau+1}^-})\omega_{\tau+1}^- - \\ &\quad M_{\tau+1}\tilde{\Pi}_{\tau+1}h(\hat{\chi}_{\tau+1}^-, u_{\tau+1}) - M_{\tau+1}\varsigma_{\tau+1}, \end{aligned} \tag{26}$$
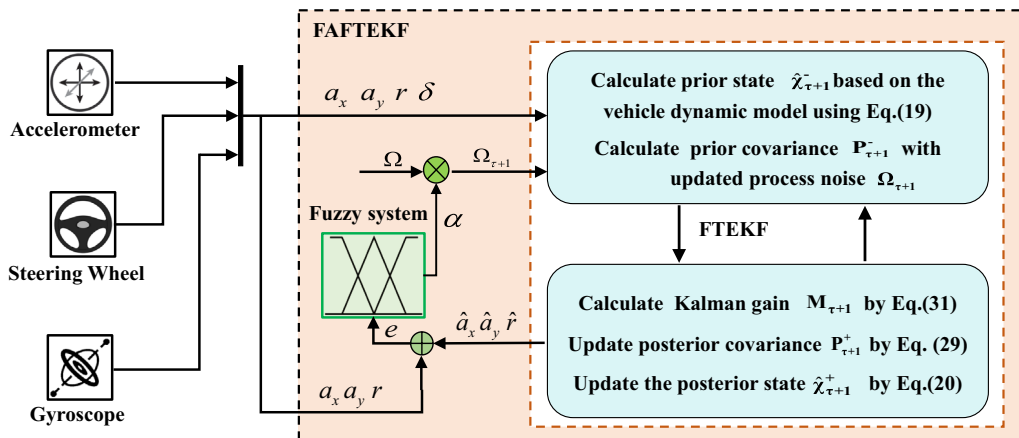

Figure 2 The flowchart of vehicle state estimation using the FAFTEKF

Zhang *et al. Chinese Journal of Mechanical Engineering* (2024) 37:118

Page 5 of 12

where $\tilde{\Pi}_{\tau+1} = \Pi_{\tau+1} - \overline{\Pi}_{\tau+1}$.

According to Eq. (24), the prior covariance $P_{\tau+1}^-$ can be expressed as Eq. (27).

$$
P_{\tau+1}^- = E\left[\omega_{\tau+1}^-\left(\omega_{\tau+1}^-\right)^{\mathrm{T}}\right]
$$
$$
= \left.\frac{\partial \Gamma(\chi_\tau, u_\tau)}{\partial \chi_\tau}\right|_{\chi_\tau=\hat{\chi}_\tau^+} P_\tau^+ \left(\left.\frac{\partial \Gamma(\chi_\tau, u_\tau)}{\partial \chi_\tau}\right|_{\chi_\tau=\hat{\chi}_\tau^+}\right)^{\mathrm{T}} + \Omega_\tau,
\tag{27}
$$

where $(\cdot)^{\mathrm{T}}$ is matrix transpose. Referring to Eq. (26), the expression for the posterior covariance $P_{\tau+1}^+$ is as follows. Let us rewrite it as:

$$
\begin{aligned}
P_{\tau+1}^+ &= \mathrm{E}\left[\omega_{\tau+1}^+\left(\omega_{\tau+1}^+\right)^{\mathrm{T}}\right] \\
&= \mathrm{E}\Big\{\,\Big[\,(I - M_{\tau+1}\Pi_{\tau+1}\left.\frac{\partial h(\chi_{\tau+1}, u_{\tau+1})}{\partial \chi_{\tau+1}}\right|_{\chi_{\tau+1}=\hat{\chi}_{\tau+1}^-})\omega_{\tau+1}^- - \\
&\quad M_{\tau+1}\tilde{\Pi}_{\tau+1}h(\hat{\chi}_{\tau+1}^-, u_{\tau+1}) - M_{\tau+1}\varsigma_{\tau+1}\,\Big] \times \\
&\quad \Big[\,(I - M_{\tau+1}\Pi_{\tau+1}\left.\frac{\partial h(\chi_{\tau+1}, u_{\tau+1})}{\partial \chi_{\tau+1}}\right|_{\chi_{\tau+1}=\hat{\chi}_{\tau+1}^-})\omega_{\tau+1}^- - \\
&\quad M_{\tau+1}\tilde{\Pi}_{\tau+1}h(\hat{\chi}_{\tau+1}^-, u_{\tau+1}) - M_{\tau+1}\varsigma_{\tau+1}\,\Big]^{\mathrm{T}}\,\Big\},
\end{aligned}
\tag{28}
$$

where I is the identity matrix. Because $\psi_\tau, \omega_\tau, \zeta_\tau$ and $\tilde{\Pi}_{\tau+1}$ are not related to each other, Eq. (28) can be rewritten as

$$
\begin{aligned}
P_{\tau+1}^+ &= \left(I - M_{\tau+1}\Pi_{\tau+1}\left.\frac{\partial h(\chi_{\tau+1}, u_{\tau+1})}{\partial \chi_{\tau+1}}\right|_{\chi_{\tau+1}=\hat{\chi}_{\tau+1}^-}\right)P_{\tau+1}^- \times \\
&\quad \left(I - M_{\tau+1}\Pi_{\tau+1}\left.\frac{\partial h(\chi_{\tau+1}, u_{\tau+1})}{\partial \chi_{\tau+1}}\right|_{\chi_{\tau+1}=\hat{\chi}_{\tau+1}^-}\right)^{\mathrm{T}} + \\
&\quad M_{\tau+1}R_{\tau+1}M_{\tau+1}^{\mathrm{T}} + M_{\tau+1}E\left[\tilde{\Pi}_{\tau+1}h(\hat{\chi}_{\tau+1}^-, u_{\tau+1}) \times \right. \\
&\quad \left. h^{\mathrm{T}}(\hat{\chi}_{\tau+1}^-, u_{\tau+1})\tilde{\Pi}_{\tau+1}^{\mathrm{T}}\right]M_{\tau+1}^{\mathrm{T}},
\end{aligned}
\tag{29}
$$

By taking the partial derivative of $P_{\tau+1}^+$ with respect to $M_{\tau+1}$, we obtain Eq. (30).

$$
\begin{aligned}
\frac{\partial tr(P_{\tau+1}^+)}{\partial M_{\tau+1}} &= -2(I - M_{\tau+1}\Pi_{\tau+1}\left.\frac{\partial h(\chi_{\tau+1}, u_{\tau+1})}{\partial \chi_{\tau+1}}\right|_{\chi_{\tau+1}=\hat{\chi}_{\tau+1}^-})P_{\tau+1}^- \times \\
&\quad \left(\left.\frac{\partial h(\chi_{\tau+1}, u_{\tau+1})}{\partial \chi_{\tau+1}}\right|_{\chi_{\tau+1}=\hat{\chi}_{\tau+1}^-}\right)^{T}\Pi_{\tau+1}^{T} + 2M_{\tau+1} \times \\
&\quad \Big\{E\left[\tilde{\Pi}_{\tau+1}h(\hat{\chi}_{\tau+1}^-, u_{\tau+1}) \times h^{T}(\hat{\chi}_{\tau+1}^-, u_{\tau+1})\tilde{\Pi}_{\tau+1}^{T}\right]\Big\} \\
&\quad + 2M_{\tau+1}R_{\tau+1},
\end{aligned}
\tag{30}
$$

By equating Eq. (30) to zero, we can obtain the expression for the gain $M_{\tau+1}$ as follows:

$$
\begin{aligned}
M_{\tau+1} &= \left[P_{\tau+1}^-\left(\left.\frac{\partial h(\chi_{\tau+1}, u_{\tau+1})}{\partial \chi_{\tau+1}}\right|_{\chi_{\tau+1}=\hat{\chi}_{\tau+1}^-}\right)^{\mathrm{T}}\Pi_{\tau+1}^{\mathrm{T}}\right] \times \\
&\quad \Big[\Pi_{\tau+1}\left.\frac{\partial h(\chi_{\tau+1}, u_{\tau+1})}{\partial \chi_{\tau+1}}\right|_{\chi_{\tau+1}=\hat{\chi}_{\tau+1}^-} P_{\tau+1}^- \times \\
&\quad \left(\left.\frac{\partial h(\chi_{\tau+1}, u_{\tau+1})}{\partial \chi_{\tau+1}}\right|_{\chi_{\tau+1}=\hat{\chi}_{\tau+1}^-}\right)^{\mathrm{T}}\Pi_{\tau+1}^{\mathrm{T}} + R_{\tau+1} + \\
&\quad E\left(\tilde{\Pi}_{\tau+1}h(\hat{\chi}_{\tau+1}^-, u_{\tau+1}) \times h^{\mathrm{T}}(\hat{\chi}_{\tau+1}^-, u_{\tau+1})\tilde{\Pi}_{\tau+1}^{\mathrm{T}}\right)\Big]^{-1},
\end{aligned}
\tag{31}
$$

where $(\cdot)^{-1}$ is the inverse of a matrix.

The key to the ability of the FTEKF to handle data loss problems compared to traditional EKF is the use of probability density functions to describe measurement loss and embed it in the measurement transfer function. The new measurement transfer function is then used to derive new filtering equations following the iterative filtering framework that allows the calculation of the data loss term to be included in the FTEKF algorithm.

3.2 The Fuzzy Logic System

In the FTEKF, it is presumed that the process noise is constant and predetermined. However, the vehicle driving conditions are intricate, encompassing continuous turning, uphill and downhill terrains, among others. Additionally, the roads on which vehicles travel exhibit varied surfaces, including ice and snow, asphalt, and gravel. These factors can directly or indirectly influence changes in the process noise. To optimize estimation performance, we propose the integration of a fuzzy logic system that dynamically updates the process noise of the robust EKF. The updated equation Ω_τ is as follows:

$$
\Omega_{\tau,new} = \alpha(e)\Omega_{\tau,old},
\tag{32}
$$

where, e represents a vector of deviations of the actual and estimated values of the three variables: longitudinal acceleration, lateral acceleration, and yaw rate, α is a

Zhang *et al. Chinese Journal of Mechanical Engineering*   (2024) 37:118

Page 6 of 12

fuzzy factor. The range of deviations from the longitudinal acceleration is $[-2, 2]$, the range of deviations from the lateral acceleration is $[-1, 1]$, and the range of deviations from the yaw rate is $[-8, 8]$. They are partitioned into three levels: NB, Z, and PB. The domain of α is $[0.001, 0.02]$, partitioned into five levels: NB, NM, Z, PM, and PB. For the degree of membership (DOM), the DOM of the input and output variables are depicted in Figure 3, respectively.

Since there are three input variables they are categorized into three classes and thus there are 27 fuzzy rules. The basic principle of setting the rules is to reduce the process noise if the deviation is too large and vice versa. Based on the aforementioned fuzzy rules, the FTEKF is capable of adaptively updating the process noise matrix.

3.3 The Boundness of FAFTEKF

In Section 3.3, the performance of the estimator will be evaluated, and certain conditions that guarantee the expected covariance remains bounded will be established. To begin with, we introduce a lemma.

Lemma 1: [28] For any two symmetric positive matrices, $(B + D)^{-1} > B^{-1} + B^{-1}DB^{-1}$, one has

$$(B + D)^{-1} > B^{-1} + B^{-1}DB^{-1}. \tag{33}$$

Theorem 1: For the system described by Eq. (4), if there exist real constants $\underline{f}$, $\overline{f}$, $\underline{h}, \overline{h} \neq 0$, and $\underline{p}, \overline{p}, \underline{\alpha}\ \overline{\alpha}, \underline{\alpha}, \overline{\varepsilon}, \underline{\varepsilon}, \underline{q}, \overline{q}$, $\underline{r}$, $\overline{r} > 0$ such that the following inequalities are satisfied for $\tau > 0$.

$$\begin{cases} \underline{q}I \leq Q_\tau \leq \overline{q}I, & \underline{f}^2I \leq A_\tau A_\tau^T \leq \overline{f}^2I, \\ \underline{r}I \leq R_\tau \leq \overline{r}I, & \underline{h}^2I \leq C_\tau C_\tau^T \leq \overline{h}^2I, \\ \underline{\alpha} \leq \alpha(e) \leq \overline{\alpha}, & \underline{\varepsilon}I \leq \aleph \leq \overline{\varepsilon}I, \quad \underline{p} \leq p \leq \overline{p}. \end{cases} \tag{34}$$
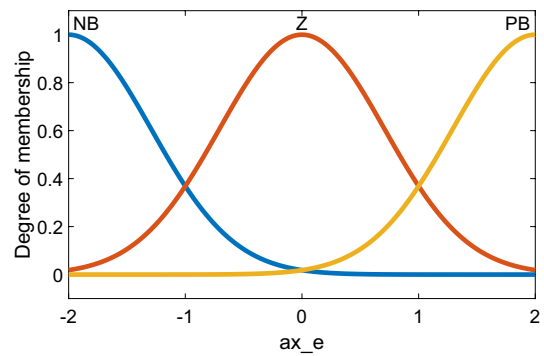
If $\lambda > 1 - \frac{1}{\overline{f}^2}$, then

$$E\left(P_{\tau+1}^-\right) \leq \overline{p}I. \tag{35}$$
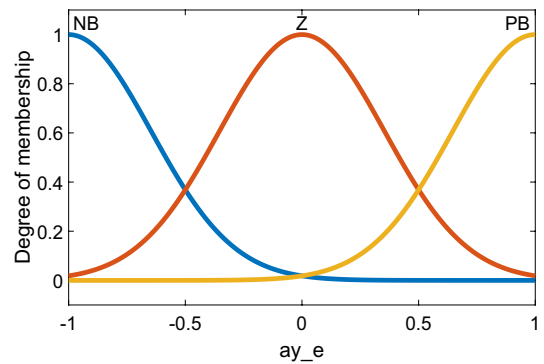
Proof: To simplify the proof process, we use the λ_τ instead of Π_τ. Therefore,

$$\begin{cases} P_{\tau+1}^+ = (I - M_{\tau+1}\lambda_{\tau+1}C_{\tau+1})P_{\tau+1}^- \times (I - M_{\tau+1}\lambda_{\tau+1}C_{\tau+1})^T + \\ \quad M_{\tau+1}R_{\tau+1}M_{\tau+1}^T + M_{\tau+1}E\left[\tilde{\Pi}_{\tau+1}h(\hat{\chi}_{\tau+1}^-, u_{\tau+1}) \times \right. \\ \quad \left. h^T(\hat{\chi}_{\tau+1}^-, u_{\tau+1})\tilde{\Pi}_{\tau+1}^T\right]M_{\tau+1}^T, \\ C_{\tau+1} = \left.\dfrac{\partial h(\chi_{\tau+1}, u_{\tau+1})}{\partial \chi_{\tau+1}}\right|_{\chi_{\tau+1}=\hat{\chi}_{\tau+1}^-} \end{cases} \tag{36}$$
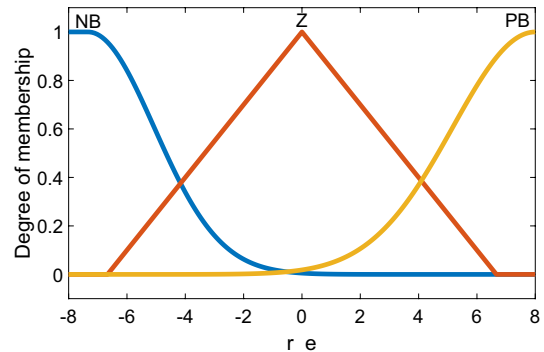
Combing Eqs. (29), (34) and the fact that $\lambda_{\tau+1}^2 = \lambda_{\tau+1}$, we have
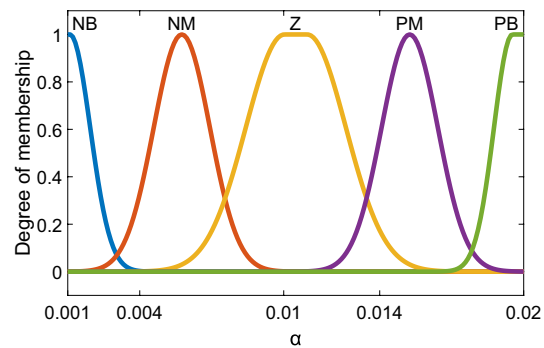

(a) The DOM of longitudinal acceleration error

(b) The DOM of lateral acceleration error

(c) The DOM of yaw rate error

(d) The DOM of α

Figure 3 The DOM of input and output variables

$$\begin{cases} P_{\tau+1}^+ = P_{\tau+1}^- - \lambda^2 P_{\tau+1}^- C_{\tau+1}^T S_{\tau+1}^{-1} C_{\tau+1} P_{\tau+1}^-, \\ S_{\tau+1} = \lambda C_{\tau+1} P_{\tau+1}^- C_{\tau+1}^T + R_{\tau+1} + \aleph, \\ \aleph = \tilde{\Pi}_{\tau+1} E\left(h(\hat{\chi}_{\tau+1}^-, u_{\tau+1}) h^T(\hat{\chi}_{\tau+1}^-, u_{\tau+1}) \right) \tilde{\Pi}_{\tau+1}^T \end{cases}$$
(37)

Based on **Lemma 1**, we have

$$P_{\tau+1}^+ \leq (1-\lambda) P_{\tau+1}^- + C_{\tau+1}^{-1}(R_{\tau+1} + \aleph) C_{\tau+1}^{-T} \quad (38)$$

Then, the prior covariance $P_{\tau+1}^-$ with adaptive process noise can be rewritten as

$$\begin{cases} P_{\tau+1}^- \leq A_\tau \left[(1-\lambda) P_\tau^- + C_\tau^{-1}(R_\tau + \aleph) C_\tau^{-T} \right] A_\tau^T + \alpha(e)\Omega_\tau, \\ A_\tau = \dfrac{\partial \Gamma(\chi_\tau, u_\tau)}{\partial \chi_\tau} \Big|_{\chi_\tau = \hat{\chi}_\tau^+}. \end{cases}$$
(39)

Combing Eqs. (34) and (39), we have

$$P_{\tau+1}^- \leq (1-\lambda) A_\tau P_\tau^- A_\tau^T + (\bar{r} + \bar{\varepsilon}) \underline{h}^{-2} A_\tau A_\tau^T + \overline{\alpha q} I,$$
(40)

$$E(P_{\tau+1}^-) \leq (1-\lambda) A_\tau E(P_\tau^-) A_\tau^T + \left[(\bar{r} + \bar{\varepsilon}) \overline{f}^2 \underline{h}^{-2} + \overline{\alpha q} \right] I.$$
(41)

At first, when $\tau = 1$, from Eq. (41), we have

$$E(P_2^-) \leq (1-\lambda) \overline{f}^2 pI + pI = p \sum_{i=0}^{1} \left\{ (1-\lambda) \overline{f}^2 \right\}^i I,$$
(42)

where $p = \max\left\{ \|E(P_1^-)\|, (\bar{r} + \bar{\varepsilon}) \overline{f}^2 \underline{h}^{-2} + \overline{\alpha q} \right\}$.

Furthermore, it is recursively proved

$$E(P_{\tau+1}^-) \leq p \sum_{i=0}^{\tau} \left\{ (1-\lambda) \overline{f}^2 \right\}^i I.$$
(43)

Thus, if $\lambda > 1 - \dfrac{1}{\overline{f}^2}$, then

$$E(P_{\tau+1}^-) \leq \overline{p} I.$$
(44)

This completes the proof.

4 Results and Discussion

The effectiveness of FAFTEKF was verified through simulation experiments and offline validation with real vehicle data, respectively. To verify the applicability of our algorithm to different working conditions and consider the safety factor, the vehicle speed is higher in the simulation experiment, while the vehicle speed is relatively lower in the real vehicle experiment.

4.1 The Simulation Results

In the test, we compared the output values from Carsim software with the estimated values obtained from the EKF, FTEKF, and FAFTEKF. The initial velocity of the vehicle is set to 50 km/h, and the vehicle is continuously steered by a virtual driver. The steering wheel angle is shown in Figure 4.

Throughout the simulation, we defined three different steering conditions. The period from 1 to 4 s represents a medium steering angle, the period from 4 to 6 s represents a large steering angle, and the period from 6 to 10 s represents a small steering angle. To simulate missing measurements, we incorporated the output values from a Bernoulli distribution with the original acceleration and yaw rate. The probability of data loss is set to 10%. As shown in Figures 5, 6, and 7, the acceleration and yaw rate abruptly change to zero at certain points, indicating that measurements were missing during those moments.

Figure 8 illustrates the estimation results for various approaches to the lateral velocity in the simulation test (ST). The vehicle state output from the Carsim software, represented by the red solid line, serves as the reference value. It can be observed that the estimated results of the EKF deviate from the reference value, as the EKF relies on all measured information being available for effective operation. On the other hand, the FTEKF demonstrates better estimation accuracy compared to the EKF because it accounts for the influence of missing measurements in its iterative process. However, the FTEKF assumes a fixed process noise, leading to decreased estimation accuracy in complex working conditions. For clearer distinction between the different algorithms for the reader, FAFTEKF is replaced by Fuzzy-FTEKF in the estimation result figures. In contrast, the FAFTEKF surpasses both the FTEKF and EKF in terms of estimation accuracy. In the FAFTEKF, a fuzzy logic system is
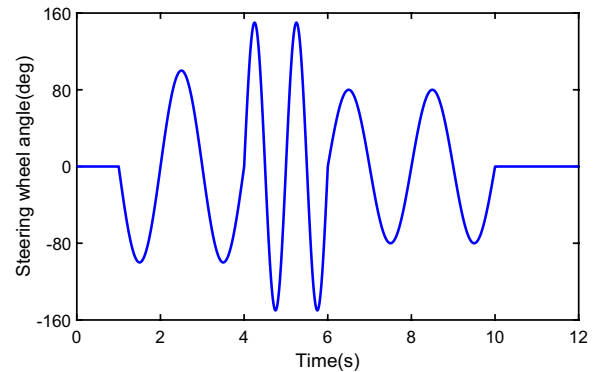

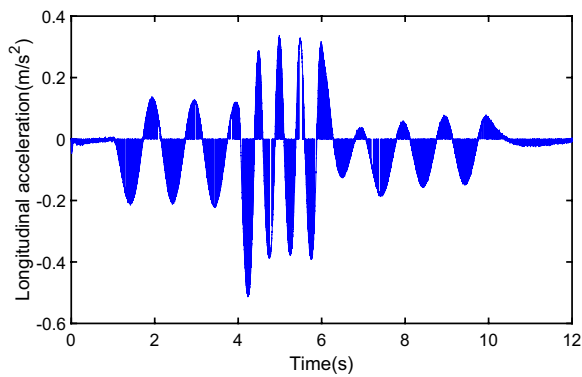**Figure 4** The steering wheel angle in the simulation test

Figure 5 Longitudinal acceleration with data loss in the ST
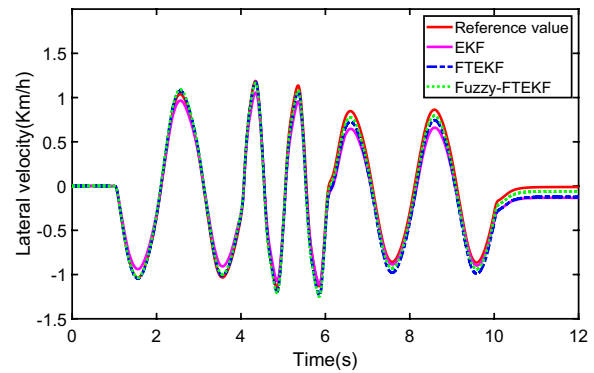

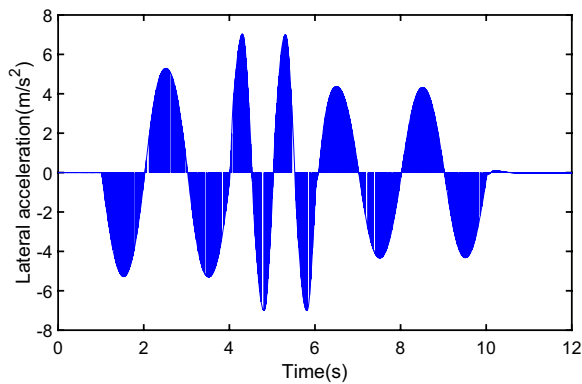**Figure 8** The estimated lateral velocity in the ST

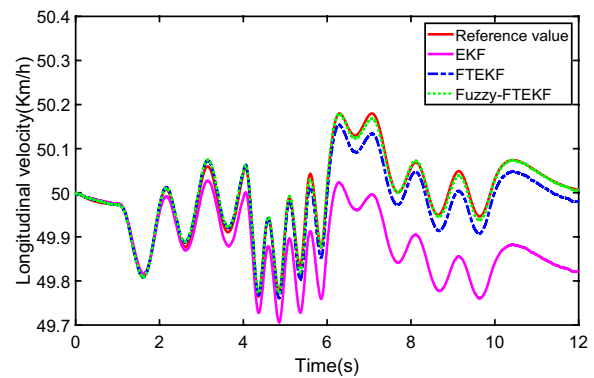**Figure 6** Lateral acceleration with data loss in the ST

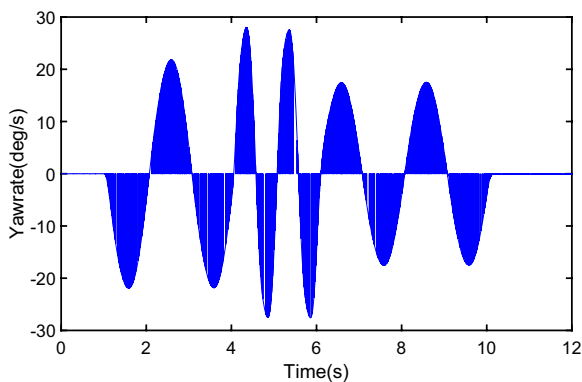**Figure 9** The estimated longitudinal velocity in the ST

Figure 7 The yaw rate with data loss in the ST

employed to dynamically adjust the process noise matrix based on lateral acceleration information. Hence, the FAFTEKF not only addresses the issue of missing measurements but also achieves adaptability in varying working conditions.

In Figure 9, the prediction results for longitudinal velocity are depicted. Similar to the estimation results for the lateral velocity, the FAFTEKF demonstrates superior performance compared to the other two methods. The proposed algorithm displays a high level of adaptability to changing driving conditions. Figure 10 depicts the estimation curves of the different methods for the sideslip angle, the estimation curve based on FAFTEKF is closest to the reference value. Figure 10 depicts the estimation curves of the different methods for the sideslip angle, the estimation curve based on FAFTEKF is closest to the reference value. To provide a clearer representation of the estimation error, the accuracy of different algorithms is showcased using the root mean square error (RMSE). Table 1 reveals that the FAFTEKF demonstrates the lowest RMSE values, indicating that the FAFTEKF achieves optimal estimation accuracy.

4.2 The Real Vehicle Test Results

To provide a more comprehensive understanding of the proposed estimation approach, we begin by collecting offline data through real vehicle tests (RVT) conducted on a dry asphalt road. The test involves a skilled
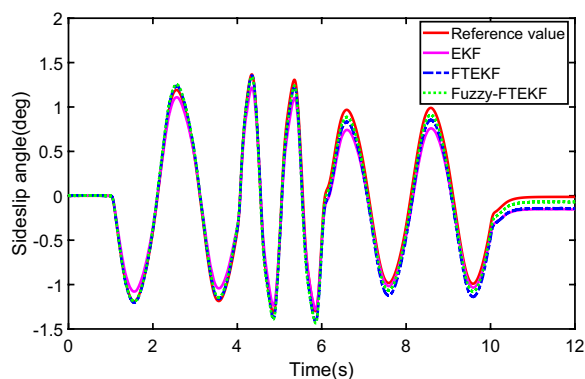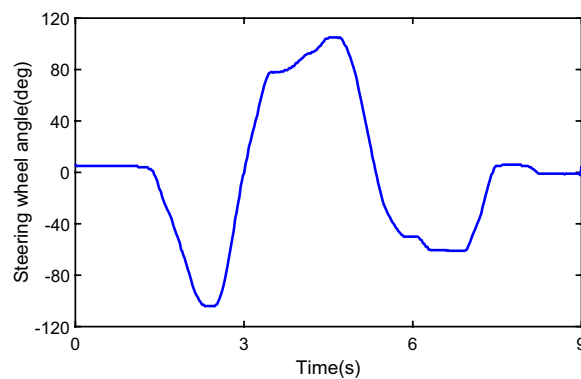
Figure 10 The estimated sideslip angle in the ST

Figure 12 The steering wheel angle in the RVT

Table 1 RMSE of vehicle state in the ST

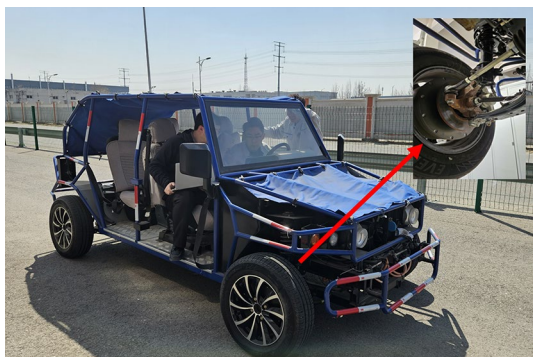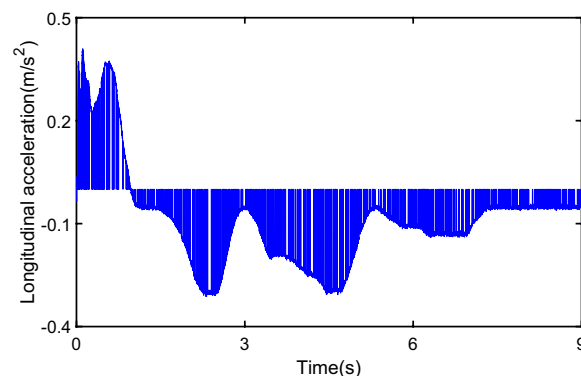| Symbol	β	v_x	v_y
EKF	0.1173	0.1323	0.1026
FTEKF	0.0996	0.0251	0.0869
FAFTEKF	0.0653	0.0071	0.0570

Figure 11 The DDEV on a dry asphalt road

Figure 13 Longitudinal acceleration with data loss in the RVT

driver performing a lane change maneuver to capture the required data. The specific test scenario is illustrated in Figure 11. Furthermore, we utilize measurements acquired from the differential global position system (DGPS) as reference values, enabling us to compare the estimation results obtained from various algorithms. The proposed algorithm is executed on a personal computer equipped with an AMD Ryzen 7 5800 HS CPU and 16.0 GB of RAM. Each cycle of the FAFTEKF algorithm takes 0.541 milliseconds to compute.

Figure 12 illustrates the variations in the front wheel angle. Compared to Figure 4, the curve representing the front wheel angle exhibits fluctuations instead of a smooth profile. This deviation originates from the

inherent limitations of human drivers, who cannot achieve perfectly smooth control akin to a machine. In Figure 13, the variations in longitudinal acceleration are depicted. Figure 14 shows the variations in lateral acceleration. In Figure 15, the variations in yaw rate are illustrated. Similarly, akin to Figures 5, 6, and 7, we replicate missing measurements by combining the output values of the Bernoulli distribution with the original acceleration and yaw rate. The probability of data loss from onboard sensors is 25%. Figures 13, 14, and 15 show abrupt drops to zero at specific points, indicating where measurements were missing.

Figure 16 illustrates the estimation results of different methods for estimating the lateral velocity. The red solid line represents the vehicle state output obtained from the DGPS, which serves as the reference value. The estimated curve produced by the EKF deviates significantly from the reference value due to its inability to handle data loss. On the other hand, the FTEKF demonstrates enhanced estimation accuracy by accounting for the impact of missing measurements. During the
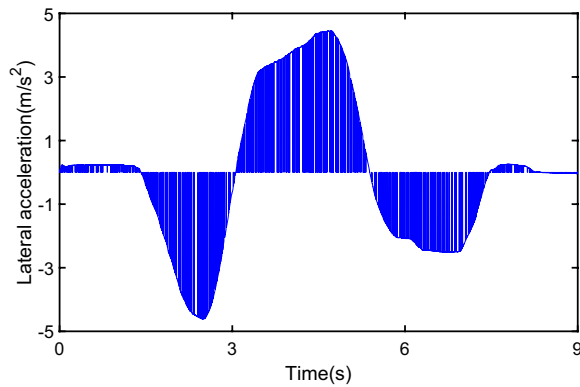
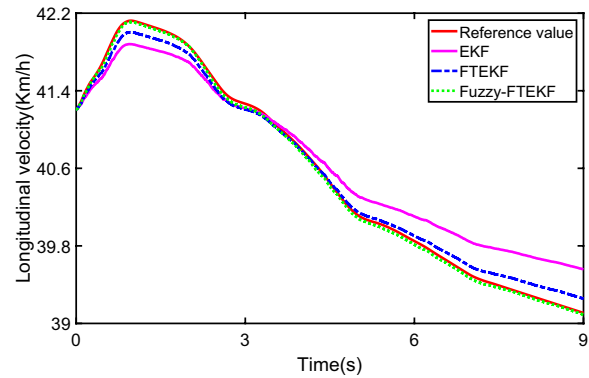**Figure 14** Lateral acceleration with data loss in the RVT

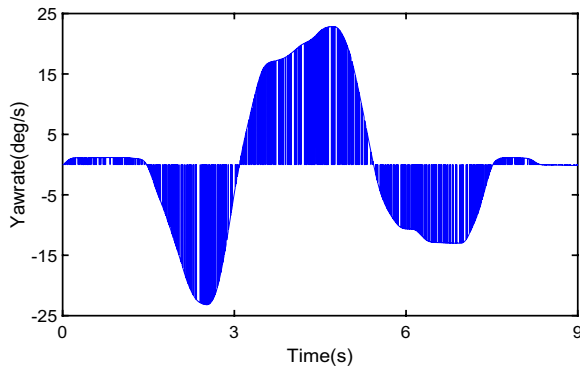**Figure 17** The estimated longitudinal velocity in the RVT

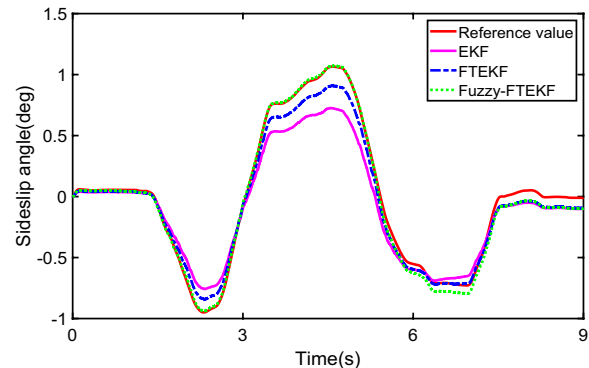**Figure 15** The yaw rate with data loss in the RVT

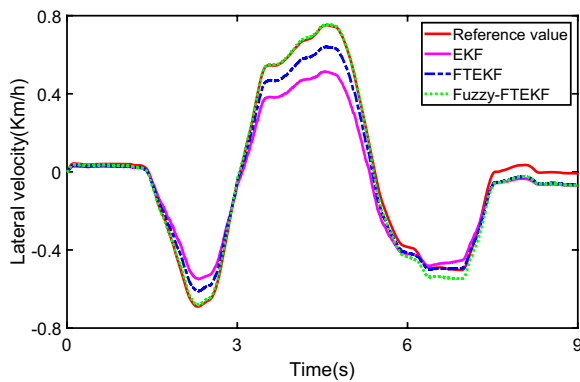**Figure 18** The estimated sideslip angle in the RVT

Figure 16 The estimated lateral velocity in the RVT

Figure 17 illustrates the prediction outcomes of various approaches for longitudinal velocity. The FAFTEKF demonstrates the highest level of accuracy in estimating longitudinal velocity compared to the other two methods. Figure 18 depicts the estimation curves of the different methods for the sideslip angle, the estimation curve based on FAFTEKF is closest to the reference value.

In Table 2, it can be observed that the FAFTEKF exhibits the lowest values for RMSE, indicating that the FAFTEKF achieves optimal estimation accuracy. These findings underscore the effectiveness of the FAFTEKF in precisely estimating both the sideslip angle and vehicle velocity. Moreover, the proposed algorithm exhibits robustness in adapting to variations in different data loss scenarios.

5 Conclusions

In this article, we have proposed the FAFTEKF as a novel approach for simultaneous estimation of sideslip angle and vehicle velocity in the presence of missing measurements. Through extensive testing, the results

conducted test, we introduce a random value as the initial process noise and then utilize a fuzzy logic system to dynamically adjust the process noise matrix. As a result, it becomes evident that the FAFTEKF outperforms the FTEKF in terms of estimation performance.

Table 2 RMSE of vehicle state in the RVT

Symbol	β	v_x	v_y
EKF	0.1562	0.2523	0.1103
FTEKF	0.0810	0.0850	0.0573
FAFTEKF	0.0492	0.0277	0.0338

demonstrate that the FAFTEKF outperforms the traditional EKF in terms of estimation accuracy. By effectively mitigating the effects of missing measurements, our proposed method showcases robustness and adaptability, particularly in response to variations in process noise. It should be noted that due to the dangers of real vehicle experiments, the vehicle speed is set to be relatively low and the speed fluctuations are kept minimal. Similarly, to demonstrate the consistency between real vehicle experiments and simulation results, the vehicle speed in the simulation scenarios also has minimal fluctuations.

Due to the limitation of some experimental sites, in the future, we will conduct more real vehicle experiments to verify the effectiveness of FAFTEKF, such as acceleration and deceleration conditions. Meanwhile, online estimation of vehicle model parameters and data loss probability distributions is also a worthy direction for future research.

Author Contributions
YW was in charge of the whole trial; ZZ wrote the manuscript; GY and CH assisted in the trial; JH, XX, and CJ conducted proofreading and made some critical revisions. All authors read and approved the final manuscript.

Availability of Data and Materials
The datasets supporting the conclusions of this article are included within the article.

Declarations

Competing Interests
The authors declare no competing financial interests.

References
[1] Y. Wang, J. Hu, F. Wang, et al. Tire road friction coefficient estimation: review and research perspectives. *Chinese Journal of Mechanical Engineering*, 2022, 35(1): 6.

[2] Z. Li, J. Hu, B. Leng, et al. An integrated of decision making and motion planning framework for enhanced oscillation-free capability. *IEEE Transactions on Intelligent Transportation Systems*, 2024, 25(6): 5718-5732.

[3] S J Scholtz , H A Hamersma. Investigating off-road vehicle lateral stability with integrated chassis control. *Vehicle System Dynamics*, 2024: 1-22.

[4] Y. Wang, H. Chen, G. Yin, et al. Motion state estimation of preceding vehicles with packet loss and unknown model parameters. *IEEE/ASME Transactions on Mechatronics*, 2023, https://doi.org/10.1109/TMECH.2023.3345956.

[5] Y. Wang, Z. Zhang, H.Wei, et al. A novel fault-tolerant scheme for multi-model ensemble estimation of tire road friction coefficient with missing measurements. *IEEE Transactions on Intelligent Vehicles.*, 2024, 9(1): 1066-1078.

[6] Y. Deng, A-T. Nguyen, C. Huang. Fault-tolerant predictive control with deep-reinforcement-learning-based torque distribution for four in-wheel motor drive electric vehicles. *IEEE/ASME Transactions on Mechatronics*, 2023, 28(2): 668-680.

[7] H. Zhang, G. Zhang, J. Wang. Sideslip angle estimation of an electric ground vehicle via finite-frequency H∞ approach. *IEEE Transactions on Transportation Electrification*, 2016, 2(2): 200-209.

[8] T. Hsiao. Robust estimation and control of tire traction forces. *IEEE Transactions on Vehicular Technology*, 2013, 62(3): 1378-1383.

[9] L. Zhao, Z. Liu, H. Chen. Design of a nonlinear observer for vehicle velocity estimation and experiments. *IEEE Transactions on Control Systems Technology*, 2011, 19(3): 664-672.

[10] X. Gao, Z. Yu, J. Neubeck et al. Sideslip angle estimation based on input-output linearization with tire-road friction adaptation. *Vehicle System Dynamics*, 2010, 48(2): 217-234.

[11] Y. Chen, Y. Ji, K. Guo. A reduced-order nonlinear sliding mode observer for vehicle slip angle and tyre forces. *Vehicle System Dynamics*, 2014, 52(12): 1716-1728.

[12] H. Imine, A. Benallegue, T. Madani, et al. Rollover risk prediction of heavy vehicle using high-order sliding-mode observer: Experimental results. *IEEE Transactions on Vehicular Technology*, 2014, 63(6): 2533-2543.

[13] T. A. Wenzel, K. J. Burnham, M. Blundell, et al. Motion dual extended Kalman filter for vehicle state and parameter estimation. *Vehicle System Dynamics*, 2006, 44(2): 153-171.

[14] G. Baffet, A. Charara, D. Lechner. Estimation of vehicle sideslip, tire force, and wheel cornering stiffness. *Control Engineering Practice*, 2009, 17(11): 1255-1264.

[15] M. Doumiati, A. C. Victorino, A. Charara, et al. Onboard real-time estimation of vehicle lateral tire-road forces and sideslip angle. *IEEE/ASME Transactions on Mechatronics*, 2011, 16(4): 601-614.

[16] K. Nam, H. Fujimoto, Y. Hori. Lateral stability control of in-wheel motor-driven electric vehicles based on sideslip angle estimation using lateral tire force sensors, *IEEE Transactions on Vehicular Technology*, 2012, 61(5), 1972-1985.

[17] F. Zhang, Y. Wang, J. Hu, et al. A novel comprehensive scheme for vehicle state estimation using dual extended H-infinity Kalman filter. *Electronics*, 2021, 10: 1526.

[18] H Tsunashima, M Murakami, J Miyataa. Vehicle and road state estimation using interacting multiple model approach. *Vehicle System Dynamics*, 2006, 44: 750-758.

[19] H. Guo, H. Chen, F. Xu, et al. Implementation of EKF for vehicle velocities estimation on FPGA. *IEEE Transactions on Industrial Electronics*, 2013, 60(9): 3823-3835.

[20] A. Katriniok, D. Abel. Adaptive EKF-based vehicle state estimation with online assessment of local observability. *IEEE Transactions on Control Systems Technology*, 2016, 24(4): 1368-1381.

[21] Y. Zhang, B. Leng, L. Xiong, et al. Distributed drive electric vehicle longitudinal velocity estimation with adaptive Kalman filter: Theory and experiment. *SAE Technical Paper*, 2019-01-0439.

[22] L. Chu, Y. Shi, Y. Zhang, et al. Vehicle lateral and longitudinal velocity estimation based on adaptive Kalman Filter. *2010 3rd International Conference on Advanced Computer Theory and Engineering (ICACTE)*. 2010, 3: V3-325-V3-329.

[23] Y. Wang, H. Wei, B. Hu, et al., Robust estimation of vehicle dynamic state using a novel second-order fault-tolerant extended Kalman filter. *SAE*

International journal of vehicle dynamics, stability, and NVH, 2023,7(3): 301-311.

[24] Y. Wang, L. Xu, F. Zhang, et al., An adaptive fault-tolerant EKF for vehicle state estimation with multiple partial missing measurements. *IEEE/ASME Transactions on Mechatronics*, 2021, 26(3): 1318-1327.

[25] Y. Wang, F. Hu, C. Tian, et al. FTEKFNet: Hybridizing physical and data-driven estimation algorithms for vehicle state. *IEEE Transactions on Intelligent Vehicles*, 2024, https://doi.org/10.1109/TIV.2024.3395911.

[26] Z. Wang, J. Wu, L. Zhang, et al., Vehicle sideslip angle estimation for a four-wheel-independent-drive electric vehicle based on a hybrid estimator and a moving polynomial Kalman smoother. *Proceedings of the Institution of Mechanical Engineers, Part K: Journal of Multi-body Dynamics*, 2018, 233(1): 125-140.

[27] J. Hu, S. Rakheja, Y. Zhang. Real-time estimation of tire-road friction coefficient based on lateral vehicle dynamics. *Proceedings of the Institution of Mechanical Engineers, Part D: Journal of Automobile Engineering*, 2020, 234(10/11): 2444-2457.

[28] S. Kluge, K. Reif, M. Brokate, et al. Stochastic stability of the extended Kalman filter with intermittent observations. *IEEE Transactions on Automatic Control*, 2010, 55(2): 514-518.

Zhiguo Zhang is currently pursuing a Ph.D. degree with the *Department of Vehicle Engineering, Southeast University, Nanjing, China*. His current research interests include vehicle state estimation and automotive active safety control.

Guodong Yin is currently a Professor at the *School of Mechanical Engineering, Southeast University, China*. He received a Ph.D. degree in vehicle engineering from *Southeast University, China*, in 2007. His current research interests include vehicle dynamics and control, connected vehicles, and multi-agent control.

Chao Huang received the Ph.D. degree in control engineering from the *University of Wollongong, Wollongong, NSW, Australia*, in 2018. She is currently a Research Assistant Professor with the *Department of Industrial and System Engineering, The Hong Kong Polytechnical University (PolyU), Hong Kong, China*. Her research interests include human–machine collaboration, fault-tolerant control, and path planning and control.

Jingyu Hu is currently working toward the Ph.D. degree at the *School of Cyber Science and Engineering, Southeast University, Nanjing, China*. His current research interests include connected vehicles, vehicle dynamics, and control and safety of Intelligent Vehicle Infrastructure Cooperative Systems.

Xing Xu received the Ph.D. degree in agricultural electrification and automation from *Jiangsu University, Zhenjiang, China*, in 2010. Since 2010, he has been with the *Automotive Engineering Research Institute, Jiangsu University, Zhenjiang, China* where he is currently a Professor. His research interests include electric and hybrid electric vehicles, energy storage systems, and advanced suspension system.

Chengyue Jiang is currently a Professor at the *School of Vehicle Engineering, Chongqing University of Technology, Chongqing, China*. His current research interests include vehicle modeling, accident reconstruction, vehicle safety, occupant protection.

Yan Wang received the Ph.D. degree in mechanical engineering from *Southeast University, Nanjing, China*, in 2022. He is currently a research associate with *The Hong Kong Polytechnical University, China*. His current research interests include vehicle system dynamics and automotive active safety control.